Bioelectrochemistry 149 (2023) 108316

Contents lists available at ScienceDirect

Bioelectrochemistry

journal homepage: www.journals.elsevier.com/bioelectrochemistry

An Oxygen-Insensitive biosensor and a biofuel cell device based on FMN L-lactate dehydrogenase

Roy Cohen [a], Nidaa S. Herzallh [a], Matan M. Meirovich [a], Oren Bachar [a], Liora Frech [a], Yifat Cohen [a], Omer Yehezkeli [a,b,c,*]

[a] Faculty of Biotechnology and Food Engineering, Technion – Israel Institute of Technology, Haifa 3200003, Israel
[b] Russell Berrie Nanotechnology Institute, Technion – Israel Institute of Technology, Haifa 3200003, Israel
[c] The Nancy and Stephen Grand Technion Energy Program Israel Institute of Technology, Haifa 3200003, Israel

ARTICLE INFO

Keywords:
Lactate biosensor
Biofuel cell
Lactate dehydrogenase
Mediated electron transfer
Direct electron transfer
Grafting

ABSTRACT

Lactate sensing has high importance for metabolic disease diagnostics, food spoilage, sports medicine, or the construction of biofuel cell devices. Therefore, continuous lactate sensing devices which enable accurate detection should be developed. Here we present the overexpression and utilization of FMN-lactate dehydrogenase from *Saccharomyces cerevisiae* for oxygen-insensitive, continuous amperometric lactate biosensing. The developed sensors exhibit a high signal-to-noise ratio, low interference effect, and a wide range of linear responses using both direct and mediated electron transfer configurations. The thionine-based mediated electron transfer configuration was stable for 8 h of continuous activity and two weeks of periodic activity with storage at 4 °C. We further grafted the redox mediators on multiwall carbon nanotubes to lower the redox mediator leaching effect. The developed grafting technique improved the biosensor stability and allowed continuous operation for at least 20 h. Both the mediator-entrapped and the grafted bioanodes were further coupled with a bilirubin oxidase-based biocathode to construct a biofuel cell device. The various biofuel cells have generated a maximal power output of 110 μW/cm^2 under atmospheric conditions and 200 μW/cm^2 under oxygen saturation.

1. Introduction

Biosensors are essential tools for accurate biomarker monitoring. Since first developed, amperometric biosensors have greatly evolved and led to improved life span and patients' quality of life. Point-of-care diagnostic devices can reduce the overall time required for physicians to recommend a treatment/medication and are therefore preferred. The revolution triggered by the development of continuous glucose monitoring devices emphasizes the importance of biomarker sensing. Lactate sensing has great significance for cancer identification and treatment [1,2], yet no intravenous (IV) or interstitial continuous sensors are currently available. The micro-environment of tumors triggers an efflux of lactate that exceeds normal levels. The increase in L-lactate concentration can be correlated with tumor metastasis, therefore its detection is highly important [3]. Interestingly, L-lactate can reach 25 mM in secreted sweat, [4] which may be utilized as an energy source or as a limiting threshold in sports medicine. Moreover, lactate biosensors use can be further extended for lactate detection in the food industry [4,5].

Currently, enzymatic lactate biosensors are mainly based on L-lactate oxidase (LOx)[6] or nicotine adenine dinucleotide- lactate dehydrogenase, (NAD-LDH) [7,8]. These enzymes oxidize lactate to pyruvate while reducing oxygen to hydrogen peroxide or NAD^+ to NADH, respectively. LOx (from *Aerococcus viridans*) is a dimer of homotetramers, where each of the 8 identical subunits contains the flavin mononucleotide (FMN) cofactor required for L-lactate to pyruvate conversion [9,10]. LOx was first conceptualized for biosensing in 1979 [11] where indirect H_2O_2 oxidation was used for lactate monitoring. Lactate sensors consisting of LOx inherently require oxygen for their activity, hence oxygen limits LOx-based biosensor accuracy. This limitation is especially important while oxygen concentration in blood or interstitial fluids fluctuates. Hypoxia is a tightly related condition that's common in metabolic diseases like diabetes or cancer. Hypoxia can also be a defining factor of tumors that may further distort the reading of LOx-based sensors. This issue can be partially addressed by the addition of proper redox mediators (second-generation biosensors), or by direct electrical communication with the electrode itself. The communication occurs via a direct

* Corresponding author.
E-mail address: y.omer@technion.ac.il (O. Yehezkeli).

https://doi.org/10.1016/j.bioelechem.2022.108316
Received 7 June 2022; Received in revised form 22 October 2022; Accepted 26 October 2022
Available online 5 November 2022

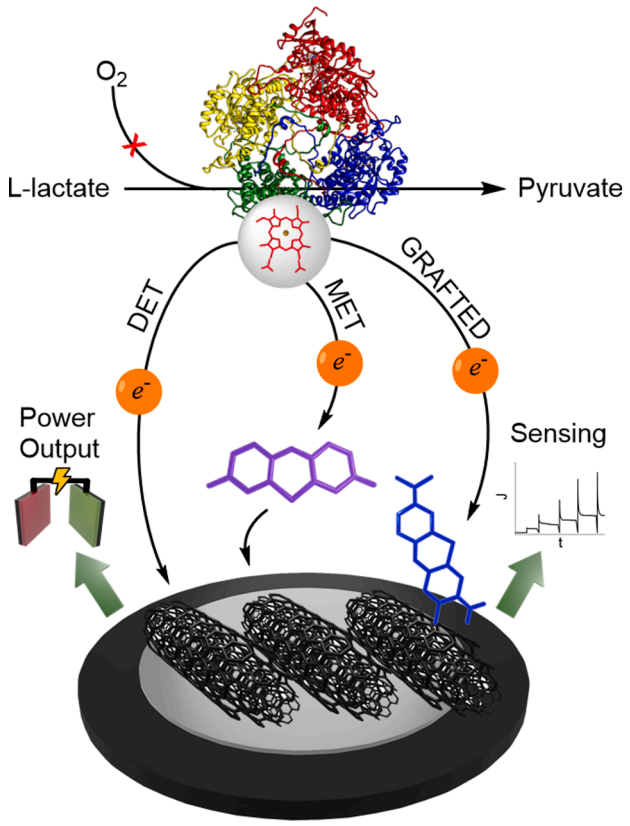

Scheme 1. A schematic description of bioanode construction. ScLDH is deposited on different types of glassy carbon electrodes for amperometric L-lactate measurement. Electrons from L-lactate oxidation can flow via three routes – direct electron transfer (I), mediated electron transfer (II), or grafted redox mediator (covalently bound, III). Bioanodes are further coupled with bilirubin oxidase biocathodes to construct biofuel cells.

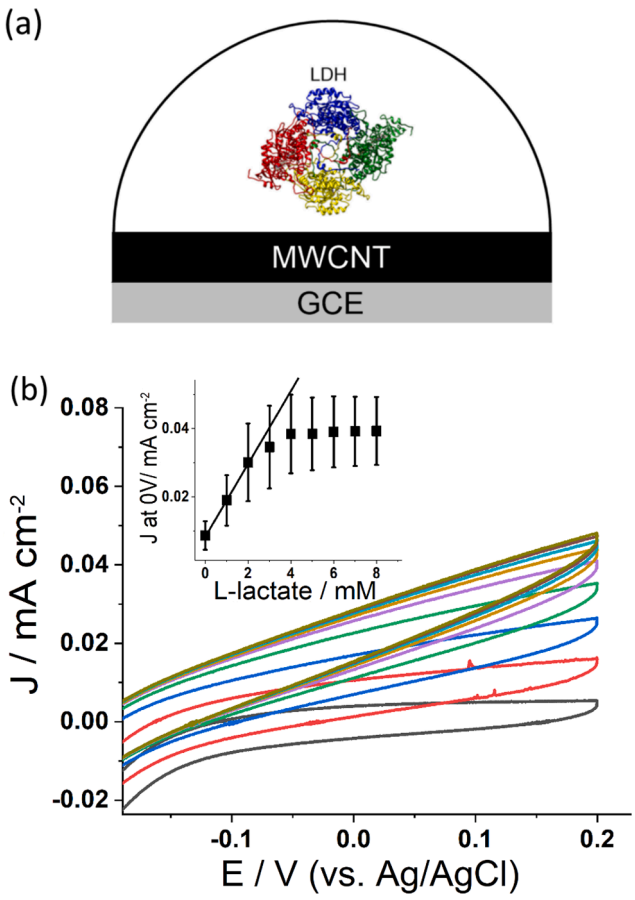

Fig. 1. Characterization of DET L-lactate bioanodes. (a) Scheme of a DET-based bioanode. ScLDH is deposited on MWCNT/GCE and incubated for one hour until complete evaporation. Afterwards, agarose is dropcasted. (b) CV measurements of DET-based ScLDH at increasing L-lactate concentrations starting at 0mM (black). The current at 0 V vs Ag/AgCl was averaged from three separate CV measurements and plotted vs [L-lactate] (inset). All CVs were performed in PB 0.1 M, pH = 7.5 at 5 mV/s.

electron transfer (DET) process that competes with oxygen, the natural electron acceptor.

Mediated electron transfer (MET) and DET configurations have been developed for the construction of amperometric lactate biosensors. Mediators such as hydroxymethylferrocene [12] or direct deposition of LOx on Nitrogen-doped carbon nanotubes [13] (CNTs) have been utilized for amperometric lactate sensing. LOx with severely reduced oxidase activity was also used in a DET configuration [14,15]. Lactate sensors have also been utilized for alcoholic beverages and dairy products monitoring [16,17]. Despite employing similar methodologies used with glucose oxidase, LOx has only seen commercial use in sensor strips to date. Recently, research advances toward continuous lactate sensing have been introduced with superior engineering toward real-time topical L-lactate sensors [18–23]. LOx-based bioanodes are also attractive for the construction of biofuel cell (BFC) devices. For that, the electrons generated by the lactate oxidation are transferred to a bilirubin oxidase (BOD) based biocathode [24,25]. Coupling these reactions generates electrical power that may be utilized for the activation of external devices, e.g. a data micro transmitter. Several key parameters are required for improved amperometric lactate sensing or lactate biofuel cell devices: (i) oxygen-independent bioanode, (ii) low onset potential for its activation, (iii) high stability and accuracy, (iv) a broad detection range.

Flavin adenine dinucleotide (FAD) dependent LDH from bacterial origins has advantages over the aforementioned LDH enzymes for sensing, however, it is a membranal protein with low stability [26]. Flavin Mononucleotide (FMN) dependent LDH (FMN-LDH) from fungi is soluble, O_2 independent, and can be overexpressed in *E. coli* [27]. FMN-LDH contains three domains – cytochrome *b*, hinge, and FMN-dependent catalytic domain. While few reports have shown its promise, continuous sensing devices or BFC applications with fungal FMN-LDH have not been presented [28–31]. Moreover, the current FMN-LDH developed amperometric biosensors have limited detection range, low microampere bioelectrocatalytic currents, and often, high overpotentials. These drawbacks limit further development of both sensing and biofuel cell applications.

Here we present the development of a new FMN-LDH-based amperometric biosensor and a lactate biofuel cell device that are both oxygen-independent. The FMN-LDH from *Saccharomyces cerevisiae* (ScLDH) was utilized for biosensing in both directed and mediated electron transfer process configurations. The developed bioanode was further coupled with a BOD-based biocathode for the development of an L-lactate/O_2 biofuel cell device. The activity of the developed biosensors was investigated in both phosphate buffer (PB) and artificial interstitial fluid (ISF) under redox potentials as low as 0 V vs Ag/AgCl. The detection limit and operational stability of the ScLDH bioanode were determined, as well as the effects of various interferents. To elucidate the enzyme-electrode electron transfer process, we overexpressed and isolated an additional variant consisting of the sole FMN-LDH catalytic subunit (lacking the heme). The different variants were examined and compared in terms of their electron transfer process capabilities and their required overpotentials. We further examined different construction methodologies for optimized bioelectrocatalytic activation of the FMN-LDH enzyme on the electrodes' surfaces. For that, different redox

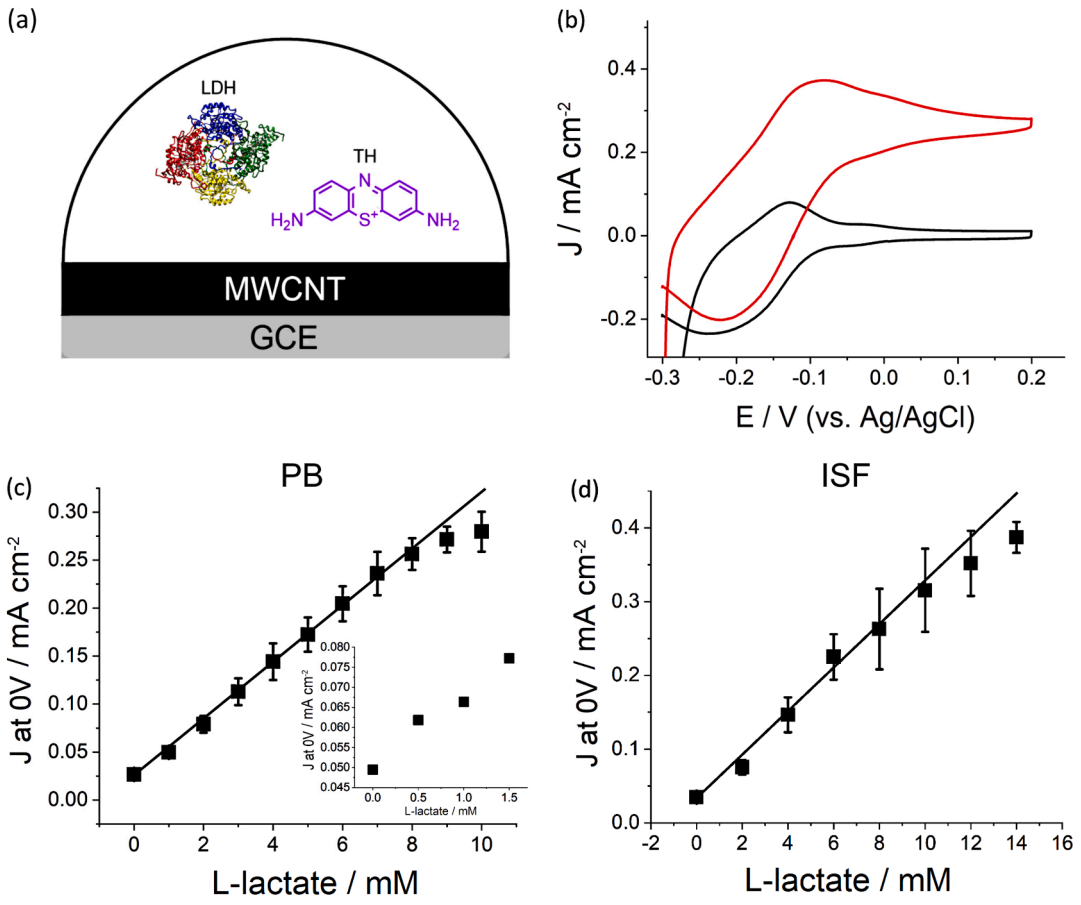

Fig. 2. Characterization of MET L-lactate bioanodes. (a) Scheme of a MET-based bioanode. ScLDH and thionine are co-deposited on MWCNT/GCE and incubated for one hour until complete evaporation. Afterwards, agarose is dropcasted. (b) CV measurements of MET-based ScLDH before (black) and after (red) addition of 8 mM L-lactate. (c) Calibration curve of amperometric L-lactate response. The current at 0 V vs Ag/AgCl was averaged from three separate CV measurements and plotted vs [L-lactate]. The inset shows measurement at low L-lactate values using the same measurement conditions. (d) MET-based calibration curve in artificial interstitial fluid (ISF) instead of phosphate buffer (PB) to simulate a fouling prone environment, see SI for further detail. The current response at 0 V vs Ag/AgCl was averaged from three CV separate measurements and plotted vs [L-lactate]. All CVs were performed in PB 0.1 M, pH = 7.5 or ISF solution at 5 mV/s.

Table 1
Comparison of L-lactate biosensors.

Enzyme type	Sensitivity ($\mu A*mM^{-1}*cm^{-2}$)	Linear detection range (mM)	Upper limit of detection (mM)	Continuous operational stability (hours)	Applied voltage vs Ag/AgCl (V)
LOx[19]	405.2	0.01–0.1	10	110	0.15 (vs SCE)
LOx[20]	3.5	0.2–1	2	N.R.	0.3
LOx[22]	0.242 ($\mu A*mM^{-1}$)	1–10	10	6	−0.1
LOx[23]	$31.2*10^{-3}$ ($\mu A*mM^{-1}$)	1–50	50	1.25	−0.05
LOx[25]	45	0–3	5	N.R.	0.3 (vs SCE)
NAD-LDH[45]	10 ($\mu A*mM^{-1}$)	$(5–90)*10^{-3}$	0.2	N.R.	0.3
b2LOxS[15]	$21*10^{-3}$	0.5–10	20	12	0.15
ScLDH[28]	10.6	0.3–2	6	N.R.	0.25
This work, ScLDH (entrapped TH configuration)	28.75	0.5–8	10	8	0
This work, ScLDH (grafted TB configuration)	63.83	1–6	14	20	0.1

*N.R.: parameter not reported.

mediators were tested while entrapment or grafting methodologies were applied. A toluidine blue (TB) grafted configuration displayed a significantly improved continuous operational stability of over 20 h. Using entrapment methodologies, the BFCs devices yielded 126 ± 2 $\mu W/cm^2$ under oxygen enrichment and 110.22 ± 2 $\mu W/cm^2$ under atmospheric conditions. By utilizing the grafting-based BFCs 157.4 ± 56 $\mu W/cm^2$ could be reached under oxygen enrichment and 78.4 ± 6 $\mu W/cm^2$ under atmospheric conditions.

2. Experimental section

For a complete description of the methods used, the reader is encouraged to view the supporting information file. The file describes enzyme sequence, additional enzyme characterization, bioanode

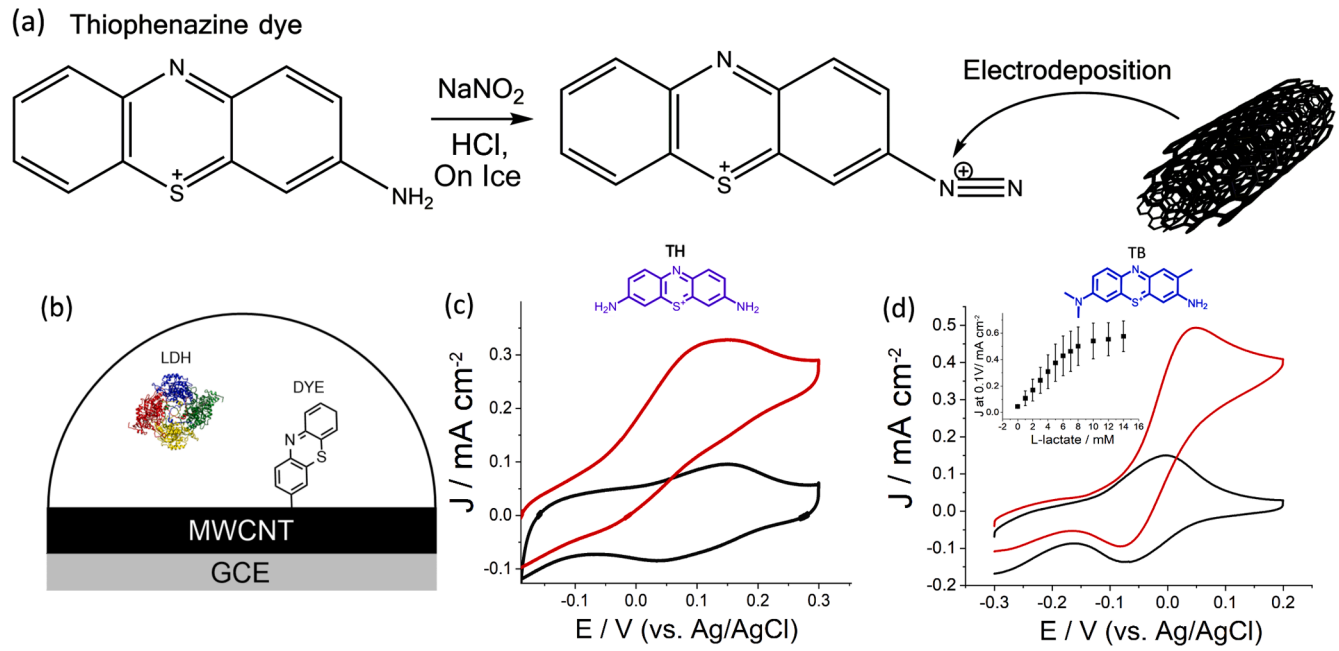

Fig. 3. Lactate sensing using the electrografting method. (a) scheme of diazonium formation and electrografting. (b) Scheme of a dye-grafted bioanode. A dye \MWCNT\GCE is formed using a diazonium dye solution, see methods section. Then, ScLDH is deposited on MWCNT/GCE and incubated for one hour until complete evaporation. Afterwards, agarose is dropcasted. (c) CV of a thionine-grafted electrode before (black) and after (red) addition of 10 mM L-lactate. (d) CV of a TB-grafted electrode before (black) and after (red) addition of 10 mM L-lactate. Inset: Amperometric response of grafted TB configuration to varying L-lactate concentration. The current response at 0 V vs Ag/AgCl was averaged from three CV separate measurements and plotted vs [L-lactate]. All CVs were performed in PB 0.1 M, pH = 7.5 at 5 mV/s.

characterization methods, and fabrication of bioanodes on alternative surfaces.

2.1. ScLDH cloning and overexpression

The *Saccharomyces cerevisiae* L-lactate Dehydrogenase (ScLDH) gene was externally synthesized and cloned into pET29b (Twist Bioscience) using the sequence from entry NP_013658.1 (NCBI), after codon optimization and removal of the signal peptide (AA 1–85). The catalytic domain of ScLDH was synthesized the same way from AAs 113–514. Competent *E. coli* BL-21 (DE3) cells were transformed with pET29ScLDH and negatively selected using kanamycin agar plates. Surviving colonies were then positively selected via colony PCR.

BL21-pET29ScLDH bacteria were grown in 100 ml of terrific broth (lacking glycerol and inoculated with 50 μg/ml kanamycin, 1 mM CaCl2, MgCl2, and 10 mM glucose). Cells were grown for 8 h (37 °C, 180RPM), induced with 0.1 mM IPTG, and grown for an additional 18 h under stirring at RT. Then, the cells were centrifuged repeatedly using a 50 ml tube until all cells were pelleted and the supernatant was removed. The cell pellet was pink due to heme production. After supernatant removal, the tube was frozen at 80 °C until further use.

2.2. ScLDH purification, SDS PAGE, absorbance, and FAD-GDH ratio

ScLDH cells from a frozen tube were resuspended in 20 ml lysis buffer (50 mM PB pH 7.5, 50 mM KCl) and disrupted by ultrasonication. Removal of cell debris was performed by centrifugation (10,000 g, 30 min', 4 °C), after which the supernatant was filtered using a 0.22μm membrane.

The supernatant was passed through an anion exchange column, then washed with 5 column volumes of the lysis buffer at 5 ml/min'. The protein was eluted using a linear gradient of 50–500 mM KCl, 50 mM PB pH = 7.5. The protein was eluted at ~ 150 mM KCl as a slightly pink solution. The eluted protein was concentrated using the Amicon 30 kDa centricons (4000RPM, 4 °C, 30 min.), then using the PALL 10 kDa centricons (4000RPM, 4 °C, 15 min'). The entire purification process was performed for both ScLDH and its catalytic domain.

The purified protein was measured via spectrophotometry. The typical absorbance of ScLDH was estimated at 2.412 for 1 mg /ml. Alternatively, the concentration of the haem b cofactor at 415 nm ($\varepsilon_{415} = 103\ mM^{-1}\ cm^{-1}$) was used to assess ScLDH concentration [32]. [haem b] was divided by [ScLDH] to yield the cofactor-protein ratio, which is indicative of purity.

For the bioanode fabrication, GCEs were polished with 1 μm and 0.05 μm alumina beads in a sequence. MWCNTs suspension (5 mg/ml) was prepared by dissolving MWCNTs in DMF, followed by sonication for 30 min'. Afterward, 5 μl of the MWCNTs solution were deposited on each GCE, which were then dried in vacuo for 30 min'.

For entrapped thionine-based bioanodes, 2 μl of thionine 20 mM and 2 μl of ScLDH 253 μM were deposited on GCE-MWCNT and dried under atmospheric conditions for one hour. Agarose was heated until boiling, then 5 μl of 1 % agarose (60 °C) was deposited on the modified GCE, which was then incubated at 4 °C for at least 30 min'.

For DET bioanodes, a GCE modified with MWCNTs was prepared as described above, then 5 μl of the ScLDH catalytic domain (65 μM) or ScLDH (253 μM) were deposited on the electrode. The electrode was dried for 30 min' under atmospheric conditions.

For grafted electrodes, thionine, NR, and TB were dissolved in acidic media, and 500ul sodium nitrite 2.4 mg/ml was added dropwise. This was incubated for at least 30 min' on ice. Two ml of the grafting stock solution were added to the electrochemical cell. Then, CV was applied (0.1V to −0.6V, 50 cycles) in order to graft the dye to the MWCNT coated GCE. Then, 4 μl of ScLDH 125 μM were deposited on top of the electrode, followed by incubation under atmospheric conditions for 30 min'. The modified GCE was then coated with agarose as mentioned above.

2.3. Bioanode saturation curve measurement

The bioanode was measured using cyclic voltammetry (CV) after a

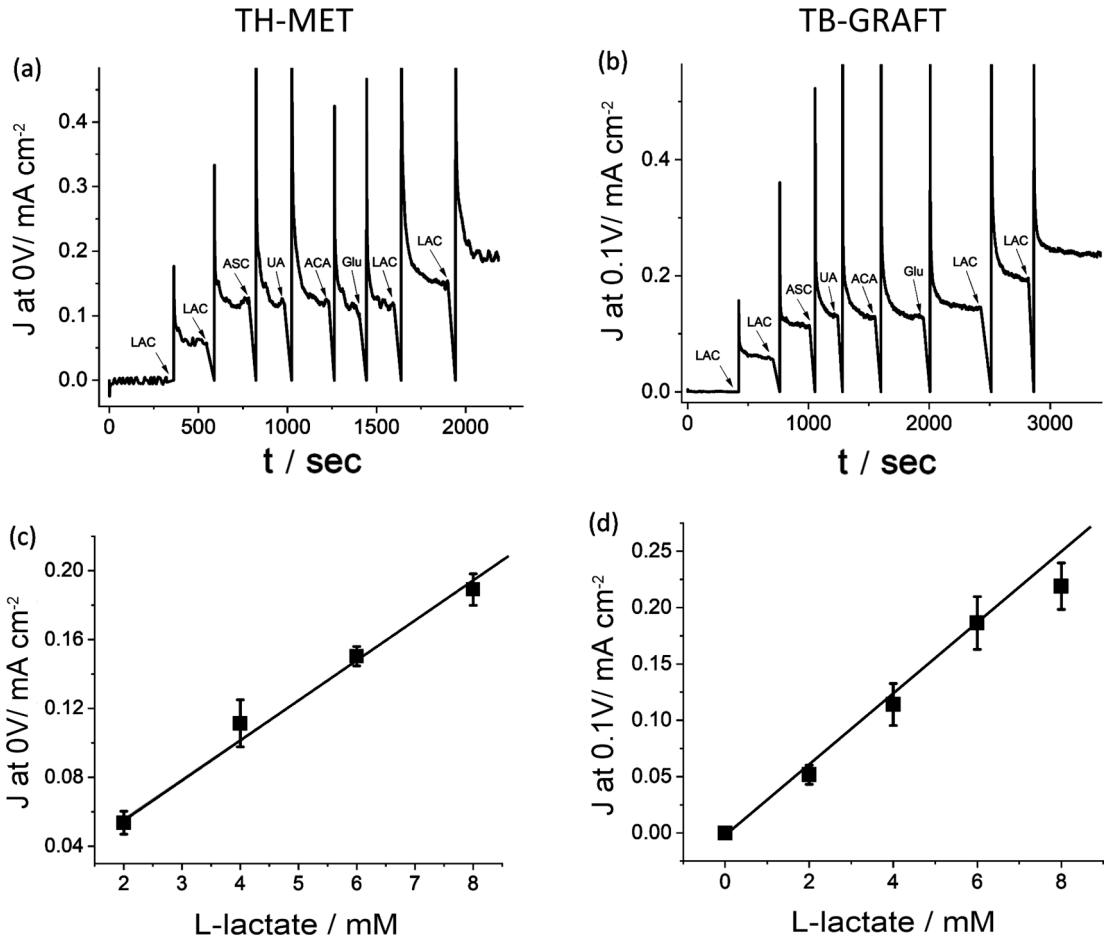

Fig. 4. Effects of interferents on L-lactate sensing. (a + b) CA measurement of common interferents of thionine-entrapped and TB-grafted configurations at 0 V or 0.1 V vs Ag/AgCl respectively. The following analytes were added in sequence from left to right: 2 mM L-lactate (twice), ascorbic acid, uric acid, acetaminophen, 50 mM glucose, 2 mM L-lactate (twice). (c + d) Linear range estimation for of thionine-entrapped and TB-grafted configurations respectively. The current of three separate CA measurements was recorded at 0 V or 0.1 V vs Ag/AgCl after each addition of lactate, then averaged and plotted vs [L-lactate].

five mins incubation period (in 20 ml PB pH = 7.5, vs Ag/AgCl, 5 mV/s). The solution was spiked with 4 mM DL-lactate (2 mM L-lactate increments), after which another CV measurement was taken until current saturation was achieved (no rise vs increasing [L-lactate]) at 0 V vs Ag/AgCl. The current at 0 V from each CV was plotted vs [L-lactate] to form the saturation curve. The same measurement was performed for the ranges of 0.5 to 1.5 mM L-lactate.

For artificial ISF measurements, the same assay was performed using an ISF-like solution composed of the following ingredients: 0.43 g Bicarbonate, 1.35 g NaCl, 1.4 g BSA, 1.9 mg Ascorbic acid, 13.7 mg uric acid, 7.2 mg fructose, 1.1 mg lactose, 53.4 mg urea, 4.8 mg calcium sulfate, and 21 mg magnesium sulfate. These salts were dissolved in 200 ml of PB 50 mM pH = 7.5.

2.4. Biocathode fabrication and measurement

For ABTS-mediated BOD biocathodes, a 5 µl mixture containing 25 mM TRIS/HCl pH 8.5, 0.8 mg/ml BOD, 0.5 mg/ml ABTS, and 0.25 mg/ml dopamine was deposited on GCE modified with MWCNTs (as described above), which was then incubated for 45 min' at RT.

Both bioanode (entrapped or grafted route) and a bilirubin oxidase biocathode were prepared as mentioned above and placed inside a triple-necked flask filled with 20 ml PB pH = 7.5 containing 20 mM DL-lactate. The cell was measured via linear sweep voltammetry (59-*sec* hold, 2 mV/s, from 0 to 0.5 V vs Eoc) using the biocathode as a reference. The measurement was taken under atmospheric conditions and O_2 enrichment.

2.5. Quantification of immobilized protein on the electrode

Two bioanodes were prepared as mentioned above, where double-distilled water was deposited onto one bioanode instead of ScLDH. Both bioanodes were soaked in 200 µl PB pH = 7.5 for one hour, after which the absorbance of each solution was measured. Both spectra were subtracted from one another to estimate the absorbance at 415 nm, yielding the desorbed [ScLDH]. This amount was subtracted from the total drop cast enzyme to yield the retained [ScLDH] on the electrode surface. The same process was repeated for all DET and MET configurations with either ScLDH or its catalytic domain.

3. Results and discussion

Initially, L-lactate Dehydrogenase (ScLDH) from *Saccharomyces cerevisiae* was cloned into *E. coli*, Fig. S1. Entry NP_013658.1 (NCBI) was used after codon optimization and signal peptide removal (residues 1–85)[27]. The full ScLDH protein including the heme, hinge, and catalytic domain, as well as the standalone FMN catalytic domain, were overexpressed. Initially, the enzymes were purified using Ni-NTA columns, however, the FMN cofactor diffused out of the protein in the presence of imidazole. Therefore, the Ni-NTA column was replaced with an anion exchange column to yield the active purified protein, Fig. S2, and Fig. S3. Various biochemical aspects of both ScLDH and the standalone catalytic domain were further characterized, Fig. S4. Then, both enzymes were used as part of direct and mediated ET configurations.

It was recently shown that heme-fused enzymes can facilitate DET

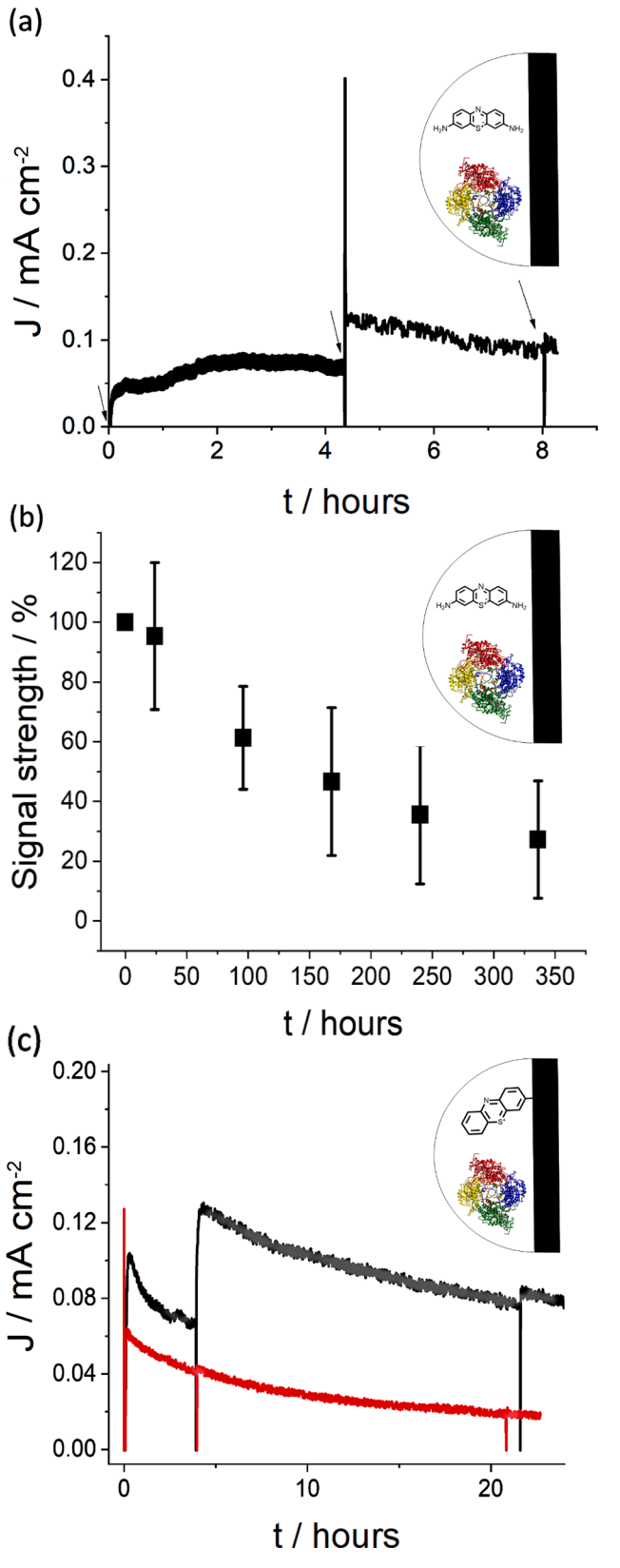

(caption on next column)

Fig. 5. Characterization of the biosensor's stability. (a) Continuous activity measurement of the thionine-entrapped configuration. A CA measurement was performed at 0 V vs Ag/AgCl. Each arrow represents the addition of 2.5 mM L-lactate at 0, 4 and 8 h. (b) Storage stability assay of the ScLDH bioanode. Three electrodes were measured using CV at fixed intervals (at 5 mV/s, see methods for further detail) before and after the addition of 5 mM L-lactate, then soaked in PB, dried, and stored at 4 °C. The current of three separate CV measurements at 0 V was averaged and normalized, then presented vs. time. (c) Continuous CA measurement of grafted thionine (red curve, at 0.2 V vs Ag/AgCl) and TB (black curve, at 0.1 V vs Ag/AgCl). Aliquots of 2.5 mM L-lactate were added at t = 0, 4, and ~ 21 h. All measurements were performed in PB 0.1 M, pH = 7.5.

processes with electrodes[15,33,34]. GOx and LOx contain an insulated FAD cofactor that is incapable of establishing efficient electrical communication with electrodes. In contrast, the ScLDH's internal heme is exposed to its surroundings. Hence, we examined if DET processes can be achieved using ScLDH. This was tested by the deposition of ScLDH onto the GCE/multiwalled-CNTs (MWCNTs) electrode, Scheme 1 route I. The GCE/MWCNTs/ScLDH electrodes were coated with boiled agarose that cooled to 60 °C. Then, the GCE/MWCNTs/ScLDH electrodes were further incubated at 4 °C for improved stability. As depicted in Fig. 1b, the ScLDH-based electrodes have shown efficient bioelectrocatalytic currents with a minute overpotential of 0.1 V. Heme redox potential is at −0.2 V [35] while the bioelectrocatalytic current onset starts at −0.1 V. For comparison, the standalone MWCNT configuration shows onset potential that correlates with lactate oxidation at 0.9 V vs Ag/AgCl, Fig. S5. We hypothesized that the FMN cofactor communicates with the electrode indirectly through the heme cofactor via an internal electron transfer process. To elucidate the electron transfer mechanism of the FMN-LDH enzyme, we overexpressed and purified the FMN catalytic subunit without the heme containing β subunit. The purified catalytic subunit was deposited on the GCE-MWCNTs electrode in a similar manner. As depicted in Fig. S6, no bioelectrocatalytic currents were obtained. These results indicate that indeed an internal electron transfer occurs in the designed configuration. The addition of a redox mediator restored the enzyme-derived bioelectrocatalytic currents, Fig. S7. These results conclude that indeed the heme cofactor is essential for DET bioelectrocatalytic process. Then, the DET-based biosensor detection range was determined. This was achieved by correlating the measured bioelectrocatalytic currents at 0 V vs Ag/AgCl to the added lactate concentrations. The generated bioelectrocatalytic currents have leveled off at ~ 27μA/cm^2, showing a linear sensing range of up to 3 mM L-lactate, Fig. 1b inset. Similar results were obtained while cyclic voltammogram measurements were replaced with chronoamperometry, Fig. S8. We further examined the scan rate vs the obtained bioelectrocatalytic currents. As presented in Fig. S9, a linear response was obtained for lactate free or lactate containing measured systems, indicating a surface confined catalyst. While the heme domain removal may lower the theoretical onset potential of activation toward the FMN redox potential (from ~ -0.2 V to ~ -0.45 V). Thus, the FMN cofactor can't establish efficient DET due to extended protein shell isolation, and therefore lacks bioelectrocatalytic activity. The linear sensing range of the DET-based configuration reached 3 mM, which is significantly higher than the average human intravenous levels (0.5–2 mM). Nevertheless, for practical biofuel cell applications or external sweat biosensors, higher currents, and an extended detection range are required. To accomplish these goals, several issues should be addressed; (i) a higher surface area, (ii) an improved orientation of the active site toward the electrode, or (iii) an improved electron transfer process using suitable redox-active molecules. Therefore, we have examined the ScLDH and its catalytic domain in a MET configuration using several redox mediators, Schematic 1 route II. The various redox mediators employed in this work are shown in Fig. S10.

First, ScLDH was co-deposited with 2,6-dichlorophenolindophenol (DCPIP) on a GCE-MWCNTs electrode. Fig. S11 depicts the

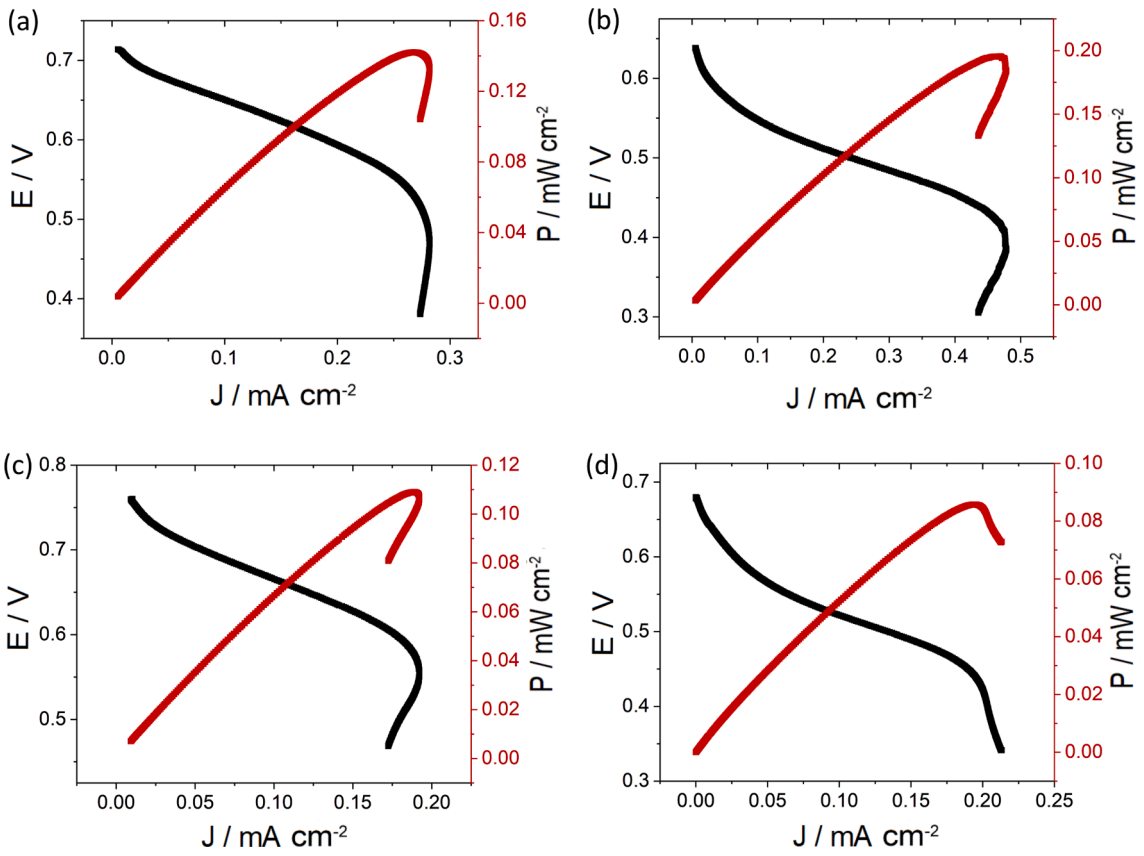

Fig. 6. Polarization curve of the ScLDH-BOD BFC. Linear sweep voltammetry was performed to measure the power output of the entrapped (a + c) or the grafted (b + d) configuration. All measurements were performed in the presence of 10 mM L-lactate and PB (0.1 M, pH = 7.5) under oxygen enrichment (a + b) or atmospheric conditions (c + d) respectively. Each measurement was repeated three times (see text for averaged power output and error margin).

Table 2
Comparison of L-lactate BFCs.

Reference and enzyme type	Open circuit voltage (V)	Max power output ($\mu W*cm^{-2}$)
LOx[25]	0.57	122
LOx[44]	0.597	113
LOx[46]	0.74	520
LOx, NAD-LDH[47]	0.9	380
This work, ScLDH (entrapped TH configuration)	0.73	126
This work, ScLDH (grafted TB configuration)	0.66	200

bioelectrocatalytic currents obtained while increasing lactate concentrations were added to the test solution. By plotting the bioelectrocatalytic currents vs lactate concentration, we could determine the linear sensing range to reach up to 1.5 mM. Furthermore, the applied potential for lactate measurement using the DCPIP configuration was above 0.1 V vs Ag/AgCl, thus, it can be influenced by common interferents. Moreover, the continuous operational stability of the DCPIP configuration lasted up to two hours, Fig. S12. To avoid the non-specific oxidation process in human body fluids, other redox mediators were considered. Redox-active mediators with lower onset potentials such as dichloro-naphthoquinone (DCNQ), anthraquinone sulfonate (AQS), methylene blue (MB), and thionine can theoretically suit the enzyme and allow activation at lower potentials. Surprisingly, while DCNQ was an excellent redox mediator in our previous work[36,37], it failed to act as a redox mediator for the ScLDH-based bioanodes. Thermodynamically, AQS and MB may act as redox mediators for the FMN cofactor positioned at the enzyme's active site (however, not for the heme cofactor). Nevertheless, both have failed to mediate the electron flux from both ScLDH and the purified FMN catalytic subunit. In contrast, the addition of thionine has enabled an efficient electron transfer process between the enzyme and the electrodes. Thionine's redox potential appears at −0.15 V vs Ag/AgCl, which is ca. 50 mV more positive than the embedded heme. It has been shown that thionine or cross-linked thionine can act as a redox mediator for GDH-based biosensors [38,39]. Therefore, thionine and purified ScLDH were entrapped in agarose gel and deposited on MWCNTs, Fig. 2a. The electrodes were further tested and the bioelectrocatalytic activity was optimized. Briefly, a glassy carbon electrode (GCE) was modified with MWCNTs followed by the addition of thionine and ScLDH (or the catalytic domain). The electrode was dried under atmospheric conditions for one hour, before the addition of the agarose-gel coating.

Then, the developed thionine-based MET bioanode was tested electrochemically using CV. As depicted in Fig. 2b, the addition of 8 mM L-lactate has led to bioelectrocatalytic currents of 0.3 mA/cm^2 at 0 V vs Ag/AgCl. The tested configuration onset potential was −0.2 V, which was dictated by the thionine redox mediator. A comparison between the developed biosensor and previous lactate sensors can be found in Table 1. Biosensors that utilize LOx and NAD-LDH possess a sensitivity below 1 $\mu A*mM^{-1}*cm^{-2}$ and\or operate at voltages above 0.1 V vs Ag/AgCl. While these parameters may suit sensing applications, the low currents and the high voltage are less attractive for biofuel cell applications. Furthermore, applied potentials above 0.1 V allow non-specific oxidation of interferents that may limit the measurement's accuracy. Then, the developed biosensor was measured repeatedly in PB while introducing increasing amounts of lactate. As shown in Fig. 2c, the developed biosensor's linear response range to lactate concentration was extended to 8 mM. Similar results were obtained while the biosensor

was tested in an artificial ISF solution, Fig. 2d. The artificial ISF contained various salts, amino acids, and significant amounts of BSA that may disrupt sensing by a fouling mechanism. We further tested the bioanode under an applied bias of 0 V vs Ag/AgCl while common interferences such as uric acid and ascorbic acid were added. As expected, no undesired oxidation reactions were observed due to the low activation potential of the enzymatic reaction dictated by thionine (ca. −0.15 V vs Ag/AgCl), Fig. 4a. The linear sensing range was conserved even in the presence of interferents, Fig. 4c. We then verified that the developed biosensor is indeed oxygen-independent by testing the electrodes under an argon atmosphere. As expected, no noticeable differences were obtained, Fig. S13. Additionally, alternative carbon surfaces were tested. This should provide a platform to develop biosensors suitable for scaled-up fabrication. As expected, the biosensor's activity on Toray paper was maintained, Fig. S14. As depicted in Fig. 3c, the current increases in response to lactate addition up to 10 mM. This configuration was applied to the sole FMN catalytic domain, Fig. S14. As depicted, the catalytic domain achieved only 70 % of the maximal current, Fig. 3c. Further measurements have concluded that DET capabilities are only possible in the presence of the heme domain, Fig. S6, and Fig. S7.

To identify key parameters such as ET rate and enzyme coverage, the ScLDH-thionine bioanode configuration was further characterized. The adsorbed amount of ScLDH and thionine on the electrode was quantified using spectrophotometry and electrochemistry to give ~ 81pmole and ~ 45nmole respectively, Fig. S15. Knowing the enzyme content on the electrode surface and the maximal bioelectrocatalytic currents generated, k_{ET} was estimated to be ~ 18 s^{-1}. Surprisingly, despite the better K_M and Vmax values obtained in the Michaelis-Menten plots, the k_{ET} of the catalytic domain lacking the heme subunit while attached to electrodes was found to be ~ 1.4 s^{-1}. We attribute these results to the higher overpotentials required for activation, both due to electrical insulation of the sole catalytic domain that lacks the heme redox bridge and poor orientation on the carbon electrodes. The stability of the ScLDH-thionine bioanode was also examined. The biosensor maintained continuous activity for at least 8 h of operation, with the current decreasing to 40 % after 8 h, Fig. 5a. We attribute the current loss to thionine leaching from the agarose layer, which occurs due to its high solubility. On the contrary, the bioanode's activity through storage cycles has shown great results. Periodic measurements of the electrodes were performed, and the electrodes were stored at 4 °C after each use. The examined electrodes-maintained response for at least two weeks, Fig. 5b. While thionine's stability is much greater than the DCPIP configuration, we examined stability-enhancing methodologies to extend the continuous operation lifetime. While the presented configurations are suitable for a short continuous measurement, long-term lactate monitoring, and biofuel cell applications both require improved operational stability. As mentioned above, the entrapped mediator limits the biosensor's long-term use due to thionine leaching. Therefore, methods to covalently integrate the redox mediator with the electrode surface should be developed. Conjugation of redox mediators with polymers backbone has been widely used for both biosensors and biofuel cell configurations [25,40]. A different approach for integration is based on a direct grafting of redox mediators on carbon surfaces, Schematic 1 route III. This approach has shown great promise while used in a glucose biosensor configuration [41]. The facile grafting method allows a simple and modular device fabrication with various redox mediators as depicted in Fig. 3a, 3b, and Fig. S16.

For that, the aromatic amine of the redox dyes was activated using in situ electrodeposition. The activation process led to the formation of a diazonium moiety, which enabled covalent attachment of the redox mediator onto the MWCNTs. Thionine was grafted successfully over the electrodes, however, the biosensor's amperometric response nearly ceased after four hours, Fig. 3c, 5c. When comparing the stability of entrapped thionine vs grafted thionine, grafting greatly improved the retention rate of the mediator from 32 % to 62 % after 12 h, Fig. S17. We, therefore, examined two additional redox mediators, neutral red (NR) and toluidine blue, (TB). Surprisingly, the NR-based biosensor didn't yield bioelectrocatalytic currents despite having an onset potential of ca. 0 V (Fig. S18). The lack of activity may stem from the incompatibility of NR with the active site, due to it being a phenazine or steric interference. On the other hand, grafted TB mediated the electron transfer process from the FMN-LDH enzyme and enabled sensing with a great linear range and improved stability, Fig. 3d, 5c. Due to grafting and the formed bonds, a potential shift of the soluble TB was apparent. As shown before [41], grafted redox molecules undergo a potential shift. Indeed, a potential shift was observed proving a successful grafting process, Fig. 3d and Fig. S19. The developed TB configuration enabled continuous L-lactate sensing with an 80 % current drop after 20 h. Examining TB-grafted bioanode interference while measuring at 0.1 V have yielded a minor response to ascorbic acid and glucose, while no response was registered for the thionine-mediated configuration, Fig. 4b, 4d. This was expected, as non-specific oxidation becomes a limitation at these voltages. Control experiments that lack the ScLDH enzyme in the GCE/MWCNTs/TB configuration did not yield any bioelectrocatalytic currents, Fig. S20. As both the entrapped and grafted configurations boosted the currents above 100uA/cm^2, they have proven suitable as bioanodes for power generation.

Therefore, entrapped and grafted bioanodes were then coupled with a previously developed bilirubin oxidase(BOD)-based biocathode to construct a biofuel cell device[42,43]. These BFC configurations generated up to 126 ± 2 μW/cm^2 under oxygen saturation and 110.2 ± 2 μW/cm^2 under atmospheric conditions, Fig. 6a and Fig. 6c. The open-circuit voltage was found to be 730 mV, which correlates with the theoretical redox values of both mediators, Fig. 2b and S21. These numbers lay with the top electrical power densities achieved using a LOx-based biofuel cell device, see Table 2. In addition to the entrapped bioanode, the grafted bioanode was also used to construct a BFC device, Fig. 6b, and Fig. 6d. The constructed BFC had reached 78.4 ± 6 μW/cm^2 under atmospheric conditions and 157.4 ± 56 μW/cm^2 under oxygen saturation. It should be noted that under atmospheric conditions, the BOD biocathode appears to be the limiting factor for power generation, yet under oxygen enrichment, this limitation is canceled. The development of lactate biofuel cells is an attractive scientific goal with many required applications. Unlike other biomarkers, lactate concentration levels are relatively high and can be detected internally or on our skin. The correlation between metabolic diseases and lactate concentration changes has been suggested, but not fully determined. Continuous monitoring of lactate could enable physicians to elucidate this broad phenomenon. Therefore, as continuous monitors become more commonly used, the next step should be a multi-sensing device that captures additional essential data. Moreover, lactate levels in sweat reach as high as 25 mM and could therefore be utilized for biofuel cell activation or battery charging. In turn, the generated electrical power could enable integrated smart devices or IoT capabilities that push the boundaries between machines and humans to the next level.

4. Conclusions

In this work, we have presented the development of an oxygen-independent, L-lactate amperometric biosensors. For that, FMN-LDH from *Saccharomyces cerevisiae* was cloned, isolated, and purified from *E. coli*. The full FNM-LDH, including the FMN catalytic and heme-containing subunits, was utilized for amperometric biosensing. The standalone catalytic domain was used as well, yet both DET and MET processes favored the full protein. The fabricated devices presented superior L-lactate detection capabilities with higher bioelectrocatalytic current at lower activation potentials as compared with previous FMN-LDH developed configurations. We investigated the enzyme-to-electrode electron transfer process and showed that both DET and MET processes can be achieved. We further show that the MET configurations reach higher bioelectrocatalytic currents with better operational stability. The bioelectrocatalytic currents reached by the developed sensors are ~

300μA/cm^2 with a linear detection ranging between 0.5 and 8 mM. This range encompasses the average L-lactate intravenous values of ~ 1 mM and most of the topical lactate range. The developed configuration can operate in both direct and mediated electron transfer processes at low overpotentials which are required for interference-free measurements. The biosensor also operates in an oxygen-independent manner to avoid the limitations of LOx-based biosensors. Additionally, a grafting methodology was implemented for improved stability. Grafted toluidine blue significantly increased the biosensor's operational stability to at least 20 h of continuous operation while maintaining a linear detection range of up to 6 mM. This greatly exceeded the operational stability of mediated configurations, which lasted several hours including both DCPIP and thionine. Both the grafted and the redox mediator entrapment configuration have presented desirable properties for future continuous amperometric lactate biosensors. The developed bioanodes were coupled with a BOD biocathode to form lactate/O_2 enzymatic biofuel cell devices. These cells yielded a maximal power output exceeding 110 μW/cm^2 under atmospheric conditions. The grafted configuration yielded lower open circuit voltage due to the ~ 200 mV onset potential shift formed in the grafting process. Even so, the grafted BFC reached up to 200 μW/cm^2 under oxygen saturation due to higher currents. The gained electrical power outputs of both configurations are similar to previously developed lactate biofuel cells[25,44]. Overall, these results show promise for grafting-based L-lactate O_2-independent sensing or energy-generating devices.

Declaration of Competing Interest

The authors declare that they have no known competing financial interests or personal relationships that could have appeared to influence the work reported in this paper.

Data availability

Data will be made available on request.

Acknowledgments

We thank the Israel Innovation Authority's Kamin program (2029940) and the Israeli Science Foundation (2029132) for providing funding and financial support.

Appendix A. Supplementary material

Supplementary data to this article can be found online at https://doi.org/10.1016/j.bioelechem.2022.108316.

References

[1] D.M. Brizel, S. Walenta, W. Mueller-Klieser, ELEVATED TUMOR LACTATE CONCENTRATIONS PREDICT FOR AN INCREASED RISK OF METASTASES IN HEAD-AND-NECK CANCER, International journal of radiation oncology, biology, physics,. 51 (2001) 349–353. https://doi.org/10.1016/s0360-3016(01)01630-3.
[2] I. San-Millán, G.A. Brooks, Reexamining cancer metabolism: lactate production for carcinogenesis could be the purpose and explanation of the Warburg Effect, CARCIN. 38 (2016) 119–133, https://doi.org/10.1093/carcin/bgw127.
[3] S. Walenta, W.F. Mueller-Klieser, Lactate: mirror and motor of tumor malignancy, Semin. Radiat. Oncol. 14 (2004) 267–274, https://doi.org/10.1016/j.semradonc.2004.04.004.
[4] M.L. Goodwin, J.E. Harris, A. Hernández, L.B. Gladden, Blood lactate measurements and analysis during exercise: a guide for clinicians, J Diabetes Sci Technol. 1 (2007) 558–569, https://doi.org/10.1177/193229680700100414.
[5] S. Liu, Practical implications of lactate and pyruvate metabolism by lactic acid bacteria in food and beverage fermentations, Int. J. Food Microbiol. 83 (2003) 115–131, https://doi.org/10.1016/S0168-1605(02)00366-5.
[6] N. Nikolaus, B. Strehlitz, Amperometric lactate biosensors and their application in (sports) medicine, for life quality and wellbeing, Microchim Acta. 160 (2008) 15–55, https://doi.org/10.1007/s00604-007-0834-8.
[7] S. Azzouzi, L. Rotariu, A.M. Benito, W.K. Maser, M. Ben Ali, C. Bala, A novel amperometric biosensor based on gold nanoparticles anchored on reduced graphene oxide for sensitive detection of l-lactate tumor biomarker, Biosens. Bioelectron. 69 (2015) 280–286, https://doi.org/10.1016/j.bios.2015.03.012.
[8] A.B. Kharitonov, M. Zayats, L. Alfonta, E. Katz, I. Willner, A novel ISFET-based NAD+-dependent enzyme sensor for lactate, Sens. Actuators B Chem. 76 (2001) 203–210, https://doi.org/10.1016/S0925-4005(01)00640-2.
[9] I. Leiros, E. Wang, T. Rasmussen, E. Oksanen, H. Repo, S.B. Petersen, P. Heikinheimo, E. Hough, The 2.1 Å structure of *Aerococcus viridans* L -lactate oxidase (LOX), Acta Cryst. 62 (2006) 1185–1190, https://doi.org/10.1107/S1744309106044678.
[10] Y. Umena, K. Yorita, T. Matsuoka, A. Kita, K. Fukui, Y. Morimoto, The crystal structure of l-lactate oxidase from Aerococcus viridans at 2.1Å resolution reveals the mechanism of strict substrate recognition, Biochem. Biophys. Res. Commun. 350 (2006) 249–256, https://doi.org/10.1016/j.bbrc.2006.09.025.
[11] L.C. Clark, [41] The hydrogen peroxide sensing platinum anode as an analytical enzyme electrode, in: Methods in Enzymology, 1979: pp. 448–479. https://doi.org/10.1016/0076-6879(79)56044-3.
[12] A.M. Parra-Alfambra, E. Casero, L. Vázquez, C. Quintana, M. del Pozo, M.D. Petit-Domínguez, MoS2 nanosheets for improving analytical performance of lactate biosensors, Sens. Actuators B Chem. 274 (2018) 310–317, https://doi.org/10.1016/j.snb.2018.07.124.
[13] J.M. Goran, J.L. Lyon, K.J. Stevenson, Amperometric detection of L-lactate using nitrogen-doped carbon nanotubes modified with lactate oxidase, Anal. Chem. 83 (2011) 8123–8129, https://doi.org/10.1021/ac2016272.
[14] K. Hiraka, K. Kojima, W. Tsugawa, R. Asano, K. Ikebukuro, K. Sode, Rational engineering of Aerococcus viridans l-lactate oxidase for the mediator modification to achieve quasi-direct electron transfer type lactate sensor, Biosens. Bioelectron. 151 (2020), 111974, https://doi.org/10.1016/j.bios.2019.111974.
[15] K. Hiraka, W. Tsugawa, R. Asano, M.A. Yokus, K. Ikebukuro, M.A. Daniele, K. Sode, Rational design of direct electron transfer type l-lactate dehydrogenase for the development of multiplexed biosensor, Biosens. Bioelectron. 176 (2021), 112933, https://doi.org/10.1016/j.bios.2020.112933.
[16] T.T. Nguyen-Boisse, J. Saulnier, N. Jaffrezic-Renault, F. Lagarde, Highly sensitive conductometric biosensors for total lactate, d- and l-lactate determination in dairy products, Sens. Actuators B Chem. 179 (2013) 232–239, https://doi.org/10.1016/j.snb.2012.10.021.
[17] S. Pérez, E. Fàbregas, Amperometric bienzymatic biosensor for l-lactate analysis in wine and beer samples, Analyst. 137 (2012) 3854, https://doi.org/10.1039/c2an35227c.
[18] M.E. Payne, A. Zamarayeva, V.I. Pister, N.A.D. Yamamoto, A.C. Arias, Printed flexible lactate sensors: design considerations before performing on-body measurements, Sci. Rep. 9 (2019) 13720, https://doi.org/10.1038/s41598-019-49689-7.
[19] P. Bollella, S. Sharma, A.E.G. Cass, R. Antiochia, Minimally-invasive microneedle-based biosensor array for simultaneous lactate and glucose monitoring in artificial interstitial fluid, Electroanalysis. 31 (2019) 374–382, https://doi.org/10.1002/elan.201800630.
[20] A. Caliò, P. Dardano, V. Di Palma, M.F. Bevilacqua, A. Di Matteo, H. Iuele, L. De Stefano, Polymeric microneedles based enzymatic electrodes for electrochemical biosensing of glucose and lactic acid, Sens. Actuators B Chem. 236 (2016) 343–349, https://doi.org/10.1016/j.snb.2016.05.156.
[21] J.R. Sempionatto, M. Lin, L.u. Yin, E. De la paz, K. Pei, T. Sonsa-ard, A.N. de Loyola Silva, A.A. Khorshed, F. Zhang, N. Tostado, S. Xu, J. Wang, An epidermal patch for the simultaneous monitoring of haemodynamic and metabolic biomarkers, Nat. Biomed. Eng. 5 (7) (2021) 737–748.
[22] H. Teymourian, C. Moonla, F. Tehrani, E. Vargas, R. Aghavali, A. Barfidokht, T. Tangkuaram, P.P. Mercier, E. Dassau, J. Wang, Microneedle-based detection of ketone bodies along with glucose and lactate: toward real-time continuous interstitial fluid monitoring of diabetic ketosis and ketoacidosis, Anal. Chem. 92 (2020) 2291–2300, https://doi.org/10.1021/acs.analchem.9b05109.
[23] X. Xuan, C. Pérez-Ràfols, C. Chen, M. Cuartero, G.A. Crespo, Lactate biosensing for reliable on-body sweat analysis, ACS Sens. 6 (7) (2021) 2763–2771.
[24] R.A. Escalona-Villalpando, R.C. Reid, R.D. Milton, L.G. Arriaga, S.D. Minteer, J. Ledesma-García, Improving the performance of lactate/oxygen biofuel cells using a microfluidic design, J. Power Sources. 342 (2017) 546–552, https://doi.org/10.1016/j.jpowsour.2016.12.082.
[25] D.P. Hickey, R.C. Reid, R.D. Milton, S.D. Minteer, A self-powered amperometric lactate biosensor based on lactate oxidase immobilized in dimethylferrocene-modified LPEI, Biosens. Bioelectron. 77 (2016) 26–31, https://doi.org/10.1016/j.bios.2015.09.013.
[26] T. Jiang, C. Gao, C. Ma, P. Xu, Microbial lactate utilization: enzymes, pathogenesis, and regulation, Trends Microbiol. 22 (2014) 589–599, https://doi.org/10.1016/j.tim.2014.05.008.
[27] M.T. Black, S.A. White, G.A. Reid, S.K. Chapman, High-level expression of fully active yeast flavocytochrome b2 in Escherichia coli, Biochem J. 258 (1989) 255–259, https://doi.org/10.1042/bj2580255.
[28] O. Smutok, M. Karkovska, R. Serkiz, B. Vus, N. Čenas, M. Gonchar, A novel mediatorless biosensor based on flavocytochrome b 2 immobilized onto gold nanoclusters for non-invasive L -lactate analysis of human liquids, Sens. Actuators B Chem. 250 (2017) 469–475, https://doi.org/10.1016/j.snb.2017.04.192.
[29] O. Smutok, G. Gayda, M. Gonchar, W. Schuhmann, A novel l-lactate-selective biosensor based on flavocytochrome b2 from methylotrophic yeast Hansenula polymorpha, Biosens. Bioelectron. 20 (2005) 1285–1290, https://doi.org/10.1016/j.bios.2004.04.020.
[30] O. Smutok, T. Kavetskyy, M. Gonchar, E. Katz, Microbial L- and D-lactate selective oxidoreductases as a very prospective but still uncommon tool in commercial

biosensors, ChemElectroChem. 8 (2021) 4725–4731, https://doi.org/10.1002/celc.202101149.
[31] S.L. Staškevičiene, N.K. Čenas, J.J. Kulys, Reagentless lactate electrodes based on electrocatalytic oxidation of flavocytochrome b2, Anal. Chim. Acta. 243 (1991) 167–171, https://doi.org/10.1016/S0003-2670(00)82555-6.
[32] A. Baudras, M. Krupa, F. Labeyrie, Molecular Complexes between Cytochrome b2 [Yeast L(+)Lactate: Cytochrome c Oxidoreductase] and Cytochrome c in the Crystalline State and in Solution, Eur J Biochem. 20 (1971) 58–64, https://doi.org/10.1111/j.1432-1033.1971.tb01362.x.
[33] I. Algov, J. Grushka, R. Zarivach, L. Alfonta, Highly efficient flavin-adenine dinucleotide glucose dehydrogenase fused to a minimal cytochrome C Domain, J. Am. Chem. Soc. 139 (2017) 17217–17220, https://doi.org/10.1021/jacs.7b07011.
[34] I. Algov, A. Feiertag, L. Alfonta, Site-specifically wired and oriented glucose dehydrogenase fused to a minimal cytochrome with high glucose sensing sensitivity, Biosens. Bioelectron. 180 (2021), 113117, https://doi.org/10.1016/j.bios.2021.113117.
[35] R.E. Sharp, S.K. Chapman, G.A. Reid, Deletions in the Interdomain Hinge Region of Flavocytochrome b2: effects on Intraprotein Electron Transfer, Biochemistry. 35 (1996) 891–899, https://doi.org/10.1021/bi950457z.
[36] R. Cohen, Y. Cohen, D. Mukha, O. Yehezkeli, Oxygen insensitive amperometric glucose biosensor based on FAD dependent glucose dehydrogenase co-entrapped with DCPIP or DCNQ in a polydopamine layer, Electrochim. Acta. 367 (2021), 137477, https://doi.org/10.1016/j.electacta.2020.137477.
[37] R. Cohen, R.E. Bitton, N.S. Herzallh, Y. Cohen, O. Yehezkeli, Utilization of FAD-Glucose Dehydrogenase from T. emersonii for Amperometric Biosensing and Biofuel Cell Devices, Anal. Chem. 93 (2021) 11585–11591, https://doi.org/10.1021/acs.analchem.1c02157.
[38] M.M. Hossain, J. Morshed, S. Tsujimura, Designing a cross-linked redox network for a mediated enzyme-based electrode, Chem. Commun. 57 (2021) 6999–7002, https://doi.org/10.1039/D1CC01707A.
[39] L. Fritea, A.J. Gross, K. Gorgy, R.K. O'Reilly, A. Le Goff, S. Cosnier, A bifunctional triblock polynorbornene/carbon nanotube buckypaper bioelectrode for low-potential/high-current thionine-mediated glucose oxidation by FAD-GDH, J. Mater. Chem. A. 7 (2019) 1447–1450, https://doi.org/10.1039/C8TA10644D.
[40] R.D. Milton, D.P. Hickey, S. Abdellaoui, K. Lim, F. Wu, B. Tan, S.D. Minteer, Rational design of quinones for high power density biofuel cells, Chem. Sci. 6 (2015) 4867–4875, https://doi.org/10.1039/C5SC01538C.
[41] S. Tsujimura, S. Tanaka, A. Gross, M. Holzinger, Electrochemical modification at multiwalled carbon nanotube electrodes with Azure A for FAD- glucose dehydrogenase wiring: structural optimization to enhance catalytic activity and stability, J. Phys. Energy. 3 (2) (2021) 024004.
[42] D. Mukha, Y. Cohen, O. Yehezkeli, BiVO4/Bilirubin Oxidase Photo(bio) electrochemical Cells for Unbiased Light-Triggered Electrical Power Generation, ChemSusChem. (2020) cssc.202000001. https://doi.org/10.1002/cssc.202000001.
[43] N.S. Herzallh, Y. Cohen, D. Mukha, E. Neumann, D. Michaeli, R. Nechushtai, O. Yehezkeli, Photosynthesis Z-Scheme biomimicry: Photosystem I/BiVO4 photo-bioelectrochemical cell for donor-free bias-free electrical power generation, Biosensors and Bioelectronics. 168 (2020), 112517, https://doi.org/10.1016/j.bios.2020.112517.
[44] I. Shitanda, Y. Morigayama, R. Iwashita, H. Goto, T. Aikawa, T. Mikawa, Y. Hoshi, M. Itagaki, H. Matsui, S. Tokito, S. Tsujimura, Paper-based lactate biofuel cell array with high power output, J. Power Sources. 489 (2021), 229533, https://doi.org/10.1016/j.jpowsour.2021.229533.
[45] M.M. Rahman, M.J.A. Shiddiky, M.A. Rahman, Y.-B. Shim, A lactate biosensor based on lactate dehydrogenase/nictotinamide adenine dinucleotide (oxidized form) immobilized on a conducting polymer/multiwall carbon nanotube composite film, Anal. Biochem. 384 (2009) 159–165, https://doi.org/10.1016/j.ab.2008.09.030.
[46] X. Chen, L. Yin, J. Lv, A.J. Gross, M. Le, N.G. Gutierrez, Y. Li, I. Jeerapan, F. Giroud, A. Berezovska, R.K. O'Reilly, S. Xu, S. Cosnier, J. Wang, Stretchable and Flexible Buckypaper-Based Lactate Biofuel Cell for Wearable Electronics, Adv. Funct. Mater. 29 (2019) 1905785, https://doi.org/10.1002/adfm.201905785.
[47] A. Koushanpour, M. Gamella, E. Katz, A Biofuel Cell Based on Biocatalytic Reactions of Lactate on Both Anode and Cathode Electrodes – Extracting Electrical Power from Human Sweat, Electroanalysis. 29 (2017) 1602–1611, https://doi.org/10.1002/elan.201700126.